Current **A**pplied **S**cience and **T**echnology e-ISSN: 2586-9396

Curr. Appl. Sci. Technol. ….., Vol... (No...), e0272301

Research article

Mathematical Modeling and Parameter Identification of Nicotine Pharmacokinetics following E-Cigarette Use

Thanachok Mahahong*

Department of Curriculum and Instruction, Faculty of Education, Nakhon Sawan Rajabhat University, Nakhon Sawan, Thailand

Received: 26 May 2026, Revised: 15 July 2026, Accepted: 28 August 2026, Published: 20 November 2026

Abstract

This study developed a five-compartment mathematical model to estimate pharmacokinetic parameters and predict nicotine distribution in unobserved tissues following modern electronic cigarette use. The model describes nicotine transport among the lungs, pulmonary blood, systemic plasma, brain, and liver using first-order ordinary differential equations incorporating volume-dependent terms to preserve mass balance. Parameter estimation via constrained optimization was performed for three platforms: Strawberry-Kiwi disposable, Tobacco disposable, and a pod-based device. The model showed excellent agreement with clinical data, achieving R^2 values of 0.9793, 0.9929, and 0.9543, with root mean square errors of 0.3651, 0.2506, and 0.2964 ng/mL, respectively. Furthermore, local sensitivity analysis demonstrated strong structural robustness, as global plasma profiles remained stable against a $\pm 20\%$ perturbation in unobserved peripheral transport parameters. Simulation results revealed distinct, device-specific tissue distribution patterns. The Strawberry-Kiwi disposable produced the highest sustained nicotine accumulation in the brain, whereas the Tobacco disposable exhibited greater hepatic accumulation following an early transient spike in brain nicotine levels. Conversely, the Pod system showed a slower, more balanced distribution profile. Overall, this framework provides a robust quantitative tool for analyzing target organ exposure and evaluating the pharmacokinetic behavior of emerging nicotine salt formulations.

Keywords: mathematical modeling; ordinary differential equations; pharmacokinetics; nicotine; e-cigarettes

*Corresponding author: E-mail: thanachok.m@nsru.ac.th
https://doi.org/10.55003/cast.2026.272301
Copyright © 2026 by King Mongkut's Institute of Technology Ladkrabang, Thailand. This is an open access article under the CC BY-NC-ND license (http://creativecommons.org/licenses/by-nc-nd/4.0/).

1. Introduction

In recent years, electronic nicotine delivery systems (ENDS) have become increasingly popular and have substantially changed patterns of nicotine consumption worldwide. Unlike conventional cigarettes, these devices generate aerosols by heating nicotine-containing liquids, with modern disposable and pod-based systems commonly using nicotine salt formulations instead of free-base nicotine. Nicotine salts are known to allow smoother inhalation and more rapid nicotine absorption, which may contribute to increased dependence potential (National Academies of Sciences, Engineering, and Medicine, 2018; Prochaska & Benowitz, 2019). As the use of these products continues to expand, understanding the pharmacokinetic behavior of nicotine across different delivery systems has become an important issue in both public health and biomedical research.

From a pharmacological perspective, several clinical studies have reported that modern nicotine salt-based electronic cigarettes can produce peak plasma nicotine concentrations ($C_{\max}$) at levels comparable to, or in some cases higher than, those observed with conventional cigarette smoking (O'Connell et al., 2019; Yingst et al., 2019a,b). Despite these findings, most experimental measurements are limited to plasma nicotine concentrations obtained from blood samples. As a result, nicotine dynamics in other physiologically important tissues, particularly the brain and liver, remain difficult to observe directly. This limitation is important because the brain is closely associated with nicotine dependence, while the liver plays a central role in nicotine metabolism and clearance (Hukkanen et al., 2005). Therefore, mathematical modeling approaches may provide a useful framework for estimating nicotine distribution in tissue compartments that cannot be measured directly in routine clinical studies.

In mathematical biology and pharmacokinetic research, compartmental modeling has long been used to describe drug absorption, distribution, and elimination processes (Godfrey, 1983; Jacquez, 1996). However, selecting an appropriate model structure remains challenging because there is often a trade-off between physiological detail and mathematical simplicity. Simpler compartmental models, such as conventional three-compartment systems (Yamazaki et al., 2010), may not fully capture the complex distribution behavior of nicotine following inhalation exposure. On the other hand, physiologically based pharmacokinetic (PBPK) models provide more detailed physiological representations (Kovar et al., 2020; Rostami et al., 2022), but they usually require a large number of parameters and substantial computational effort. In practice, this can lead to parameter identifiability difficulties, particularly when models are adapted to different electronic cigarette devices. In addition, many existing pharmacokinetic models were developed before the widespread use of modern nicotine salt products and may not adequately reflect the rapid nicotine delivery characteristics reported for contemporary disposable and pod-based systems (Robinson et al., 2018; Hajek et al., 2020; Talih et al., 2022). Therefore, there remains a need for computationally efficient mathematical models that can capture device-specific nicotine kinetics while remaining suitable for parameter estimation and predictive analysis (Hindmarsh et al., 2005; Raue et al., 2009).

Based on these limitations, the present study develops a five-compartment mathematical model to describe nicotine pharmacokinetics following the use of modern electronic cigarettes. The five-compartment structure was strategically selected as the minimal representation required to capture the full inhalation-to-elimination pathway of nicotine—spanning pulmonary deposition (C_1), arterial transfer (C_2), systemic distribution (C_3), brain uptake (C_4), and hepatic metabolism (C_5). This architecture isolates key

targets of addiction (brain) and clearance (liver), avoiding the mathematical over-parameterization and identifiability challenges common in full-scale PBPK models while offering superior tissue-level resolution over traditional 2- or 3-compartment systems (Hukkanen et al., 2005; Rostami et al., 2022). Using high-resolution clinical plasma nicotine data reported by Falarowski et al. (2025), this study focuses on two main objectives: first, to estimate pharmacokinetic rate constants through a constrained optimization approach, and second, to reconstruct nicotine distribution in tissue compartments that cannot be directly measured in routine clinical studies. By combining mathematical modeling with clinical data, the proposed framework aims to provide further insight into how different electronic cigarette devices may influence systemic nicotine exposure and tissue-level nicotine dynamics.

2. Materials and Methods

2.1 Mathematical model formulation

A five-compartment pharmacokinetic model was developed to describe nicotine distribution following inhalation from electronic cigarette devices. The model represents the body as a system of interconnected compartments corresponding to major physiological regions involved in nicotine transport and clearance, consistent with established nicotine pharmacokinetic studies (Hukkanen et al., 2005). To maintain both biological relevance and mathematical simplicity, the model was formulated in terms of compartmental nicotine concentrations $C_i(t)$ (ng/mL) rather than total nicotine mass. This formulation allows direct comparison with clinical plasma concentration data and naturally accounts for differences in compartment volumes during nicotine transfer between tissues.

A key feature of the proposed model is the inclusion of compartment volume ratios, $\left(v_i / v_j\right)$, within the transfer terms to preserve mass balance between compartments with different physiological volumes (Ynineb et al., 2025). This formulation ensures that nicotine leaving one compartment corresponds consistently to the amount entering another compartment after accounting for volume differences. The model considers five functional compartments involved in nicotine transport and disposition: C_1 (lung), C_2 (pulmonary blood), C_3 (systemic plasma), C_4 (brain), and C_5 (liver). While other physiologically relevant organs like the heart play roles in systemic circulation, they were excluded from the explicit model structure. Because the heart is neither a major nicotine reservoir nor a primary metabolic site, nicotine passes through cardiac tissues rapidly without significant accumulation or clearance (Hukkanen et al., 2005). Therefore, to maintain mathematical parsimony and avoid over-parameterization, perfusion-limited tissues (e.g., heart, kidneys, and muscles) were implicitly lumped into the systemic plasma compartment, allowing a dedicated focus on the primary target of addiction (brain) and the principal site of clearance (liver).

Physiological compartment volumes v_i were approximated using the standard adult reference values reported in previous studies (Davies & Morris, 1993; Price et al., 2003): $V_3 = 4.0$ L, $V_4 = 1.4$ L, and $V_5 = 1.8$ L. Nicotine movement between compartments is described using first-order transfer rate constants (min^{-1}), which represent the rate of nicotine transport from compartment *i* to compartment *j*. A schematic representation of the compartmental structure used in this study is shown in Figure 1.

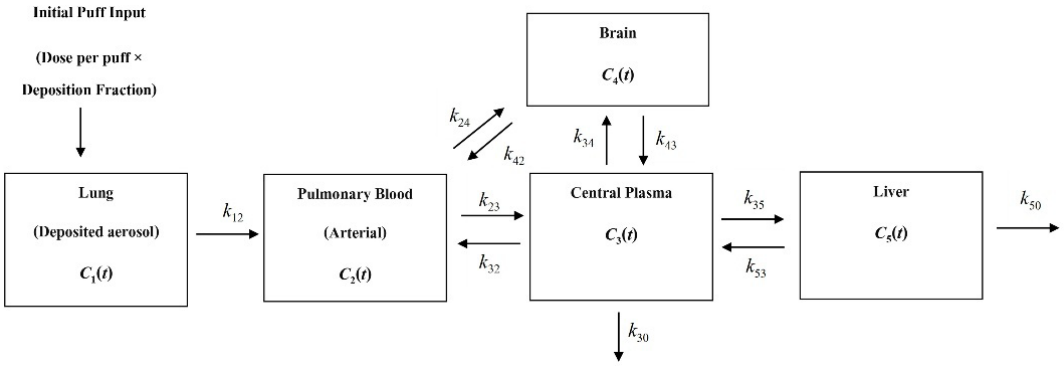


Figure 1. Schematic representation of the five-compartment model for nicotine pharmacokinetics, illustrating the fluxes (k_{ij}) between the lung, pulmonary blood, systemic plasma, brain, and liver

Using the law of mass action and assuming that each compartment is well-mixed with first-order transfer kinetics, the nicotine transport dynamics between compartments are described by the following system of linear ordinary differential equations (ODEs):

$$\frac{dC_1(t)}{dt} = -k_{12}C_1(t), \tag{1}$$

$$\frac{dC_2(t)}{dt} = k_{12}\frac{v_1}{v_2}C_1(t) + k_{32}\frac{v_3}{v_2}C_3(t) + k_{42}\frac{v_4}{v_2}C_4(t) - \left(k_{23} + k_{24}\right)C_2(t), \tag{2}$$

$$\frac{dC_3(t)}{dt} = k_{23}\frac{v_2}{v_3}C_2(t) + k_{43}\frac{v_4}{v_3}C_4(t) + k_{53}\frac{v_5}{v_3}C_5(t) - \left(k_{32} + k_{34} + k_{35} + k_{30}\right)C_3(t), \tag{3}$$

$$\frac{dC_4(t)}{dt} = k_{24}\frac{v_2}{v_4}C_2(t) + k_{34}\frac{v_3}{v_4}C_3(t) - \left(k_{42} + k_{43}\right)C_4(t), \tag{4}$$

$$\frac{dC_5(t)}{dt} = k_{35}\frac{v_3}{v_5}C_3(t) - \left(k_{53} + k_{50}\right)C_5(t). \tag{5}$$

In this model, the rate constants k_{ij} represent specific physiological transport processes. The parameter k_{12} describes nicotine absorption from the lungs into the pulmonary blood compartment, while k_{23} and k_{32} represent the bidirectional exchange between pulmonary blood and systemic plasma. Nicotine transport between the circulatory system and the brain is described by k_{24}, k_{42} and k_{34}, k_{43}, which account for nicotine uptake into and redistribution from the brain compartment. Similarly, k_{35} and k_{53} characterize nicotine exchange between systemic plasma and the liver compartment. The

elimination terms k_{30} and k_{50} correspond to first-order nicotine clearance from the systemic plasma and liver compartments, respectively.

The initial conditions assume that the inhaled nicotine dose D is deposited rapidly into the lung compartment $t = 0$:

$$C_1(0) = \frac{D}{V_1},\ C_i(0) = 0 \text{ for } i = \{2,3,4,5\} \tag{6}$$

where D is the total effective mass of nicotine delivered to the lower respiratory tract, yielding initial lung concentrations ($C_1(0)$) of 41.67 ng/mL for the Strawberry-Kiwi disposable, 46.67 ng/mL for the Tobacco disposable, and 20.00 ng/mL for the Pod System (Myblu).

2.2 Clinical data and model calibration

The proposed model was calibrated using plasma nicotine concentration data reported by Falarowski et al. (2025). The dataset consisted of arithmetic mean plasma nicotine concentrations corresponding to the systemic plasma compartment, C_3, which were obtained by digitizing Figure 1a from the original study. Blood samples in the clinical study were collected at nine time points following inhalation exposure.

Three electronic nicotine delivery systems (ENDS) with different nicotine delivery characteristics were included in the analysis: a Strawberry-Kiwi disposable device (Elf Bar 600), a Tobacco disposable device (Elf Bar 600), and a pod-based system (Myblu). The digitized plasma nicotine concentrations used for model calibration are summarized in Table 1.

For comparison with the original clinical study, the reported pharmacokinetic summary parameters were also considered. Falarowski et al. (2025) reported geometric mean peak plasma concentrations (C_{max}) of 7.1, 6.9, and 3.1 ng/mL, time-to-peak concentrations (T_{max}) of 5, 6, and 6 min, and area under the concentration-time curve from 0–30 min (AUC_{0-30}) values of 111.3, 110.6, and 58.3 ng/mL·min for the Strawberry-Kiwi disposable, Tobacco disposable, and Pod system, respectively.

Building upon the concentration–time data presented in Table 1, the effective nicotine dose (D) for each device was estimated using the labeled nicotine concentration of the e-liquid (20 mg/mL for the disposable devices and 18 mg/mL for the Myblu pod system), the average number of puffs reported during use (approximately 17 puffs), the mean puff volume (approximately 80 mL for the disposable devices and 76 mL for the Myblu system), and an assumed pulmonary deposition fraction consistent with previous studies on nicotine salt aerosol inhalation (Rostami et al., 2022). These estimated doses were used to define the initial condition of the lung compartment at $t = 0$. By assuming rapid nicotine deposition in the lung compartment immediately after inhalation, the model provides a standardized baseline for comparing nicotine transport dynamics across different electronic cigarette devices. This approach allows the influence of device-specific kinetic behavior on nicotine distribution to be evaluated more consistently.

Table 1. Clinical plasma nicotine concentration (arithmetic mean and 95% confidence interval (CI)) (ng/mL) (Falarowski et al., 2025).

Time (min)	Disposable (Straw-Kiwi)	Disposable (Tobacco)	Pod System (Myblu)
0	0.0	0.0	0.0
1	5.3	4.0	0.3
2	8.0	9.3	1.0
4	7.8	9.4	3.2
6	8.4	8.5	4.1
8	6.7	6.3	3.5
10	5.6	5.5	3.0
12	5.5	4.5	2.9
30	3.0	2.8	2.3
Total Dose (D)	50 mg	56 mg	24 mg

Note: Arithmetic mean peak values exceed the published geometric mean C_{max} (7.1, 6.9, and 3.1 ng/mL for strawberry-kiwi, tobacco, and pod system, respectively) due to high inter-subject variability (CV = 141–168%). Arithmetic mean profiles were used for ODE calibration to preserve temporal dynamics at each discrete sampling point.

2.3 Parameter estimation and computational implementation

Model parameter estimation was formulated as a nonlinear least-squares optimization problem (Aster et al., 2018). The objective of the optimization procedure was to minimize the difference between the simulated nicotine concentration in the systemic plasma compartment, $C_3(t)$, and the corresponding clinical plasma nicotine data. To quantify the fitting error, the following objective function $J(\theta)$ was defined as:

$$J(\theta) = \sum_{m=1}^{M} \left(C_3(t_m, \theta) - y_m \right)^2$$

where y_m denotes the experimental nicotine concentration at time t_m, and $\theta = [k_{12}, k_{23}, ..., k_{50}]^T \in \mathbb{R}^{11}$ is the vector of unknown kinetic rate constants.

The numerical implementation of the proposed model was carried out in MATLAB. The system of ordinary differential equations was solved using the ode45 solver, an adaptive fourth–fifth order Runge–Kutta method, with relative and absolute error tolerances specified to ensure numerical stability and accuracy. Model calibration was performed using the lsqcurvefit function with the trust-region-reflective optimization algorithm (Raue et al., 2009). The optimization procedure was configured with a predefined function tolerance and a maximum of 20,000 function evaluations.

All eleven model parameters (k_{ij}) were estimated simultaneously under physiologically reasonable box constraints, as summarized in Table 2. These lower and upper bounds were strategically differentiated based on biophysical principles, rather than uniformly set, to ensure that the parameter identification process yielded biologically meaningful results. Specifically, the pulmonary absorption rate (k_{12}) was initialized at 1.5

min^{-1} and constrained within the range of 0.5 to 5.0 min^{-1} to reflect the ultra-fast absorption of nicotine salt aerosols (Rostami et al., 2022). Similarly, the brain influx rates (k_{24} and k_{43}) were assigned relatively high upper bounds (up to 5.0 min^{-1}) because nicotine crosses the blood–brain barrier rapidly due to its high lipophilicity (Hukkanen et al., 2005), closely mimicking the rapid arterial bolus effect observed in combustible cigarette smoking. In contrast, the systemic distribution rates (k_{32} , k_{34} and k_{42}) and elimination/hepatic clearance parameters (k_{30} and k_{50}) were bounded within tighter, physiologically realistic windows (0.005 to 1.5 min^{-1}). These bounds were aligned with the reported human plasma half-life of nicotine, standard clearance capacities, and organ perfusion constraints documented in established pharmacokinetic literature (Hukkanen et al., 2005; Benowitz et al., 2009; St. Helen et al., 2016). Implementation of these non-uniform boundaries prevents the non-linear least-squares algorithm from exploring mathematically trivial but biologically implausible domains, such as negative values or infinitely large transfer rates, thereby ensuring that the calibrated model adheres strictly to systemic mass balance constraints.

Table 2. Initial parameter values and physiologically constrained lower and upper bounds used for estimating the eleven kinetic rate constants in the proposed pharmacokinetic model.

Parameters	θ	Lower Bound (lb)	Upper Bound (ub)	unit
k_{12}	1.500	0.500	5.000	min^{-1}
k_{23}	0.100	0.010	1.000	min^{-1}
k_{32}	0.050	0.010	1.000	min^{-1}
k_{30}	0.010	0.005	0.100	min^{-1}
k_{24}	1.000	0.010	5.000	min^{-1}
k_{42}	0.010	0.005	1.000	min^{-1}
k_{34}	0.150	0.010	2.000	min^{-1}
k_{43}	0.010	0.005	1.000	min^{-1}
k_{35}	1.000	0.010	2.000	min^{-1}
k_{53}	0.100	0.005	2.000	min^{-1}
k_{50}	0.050	0.005	1.000	min^{-1}

The goodness-of-fit between the simulated and observed plasma nicotine concentrations was evaluated using the coefficient of determination (R^2) and the root mean square error (*RMSE*).

3. Results and Discussion

3.1 Parameter identification and kinetic characterization

The first objective of this study was achieved by solving a nonlinear least-squares inverse problem to estimate the eleven kinetic rate constants (θ). The optimized parameter values, together with the statistical measures used to assess model performance, are summarized

in Table 3. These parameters describe the rates of nicotine transfer (k_{ij}) between physiological compartments and reflect the distinct pharmacokinetic characteristics associated with each electronic cigarette delivery system investigated in this study.

The model showed good agreement with the clinical plasma nicotine data across all three electronic cigarette platforms, as illustrated in Figures 2 and 3. Among the evaluated devices, the Tobacco disposable system produced the highest fitting accuracy (R^2 = 0.9929, *RMSE* = 0.2506 ng/mL), followed by the Strawberry-Kiwi disposable (R^2 = 0.9793, *RMSE* = 0.3651 ng/mL) and the Pod system (R^2 = 0.9543, *RMSE* = 0.2964 ng/mL). These results indicate that the proposed five-compartment ODE model was able to reproduce the characteristic nicotine absorption and distribution profiles observed in the clinical data for each device type.

Table 3. Optimized kinetic rate constants (k_{ij}, min^{-1}) and goodness-of-fit statistics obtained for the three electronic nicotine delivery systems (ENDS) evaluated in this study.

Time (min)	Disposable (Straw-Kiwi)	Disposable (Tobacco)	Pod System (Myblu)
k_{12}	5.0000	1.7330	0.5291
k_{23}	0.7896	0.0100	0.5123
k_{32}	0.0470	0.0262	0.0100
k_{30}	0.0050	0.0050	0.0050
k_{24}	0.1007	2.1351	0.0100
k_{42}	0.0066	0.0050	0.0679
k_{34}	0.0587	0.0050	0.0921
k_{43}	0.0155	2.0000	0.0100
k_{35}	0.0100	0.1322	0.0100
k_{53}	0.0211	0.0371	0.0674
k_{50}	0.0050	0.0050	0.0050
R^2	0.9793	0.9929	0.9543
RMSE	0.3651	0.2506	0.2964

The estimated pulmonary absorption rate constant (k_{12}) differed noticeably among the three electronic cigarette platforms. The Strawberry-Kiwi disposable device showed the highest absorption rate (k_{12} =5.0000 min^{-1}), suggesting very rapid nicotine transfer from the lung compartment into the pulmonary circulation. The Tobacco disposable device also exhibited relatively fast pulmonary absorption (k_{12} = 1.7330 min^{-1}), although at a lower rate than the Strawberry-Kiwi device. In contrast, the Pod system demonstrated a slower pulmonary uptake profile (k_{12} = 0.5291 min^{-1}). These differences in pulmonary absorption kinetics may be associated with variations in aerosol generation, nicotine salt formulation, and device power characteristics among the evaluated electronic cigarette systems.

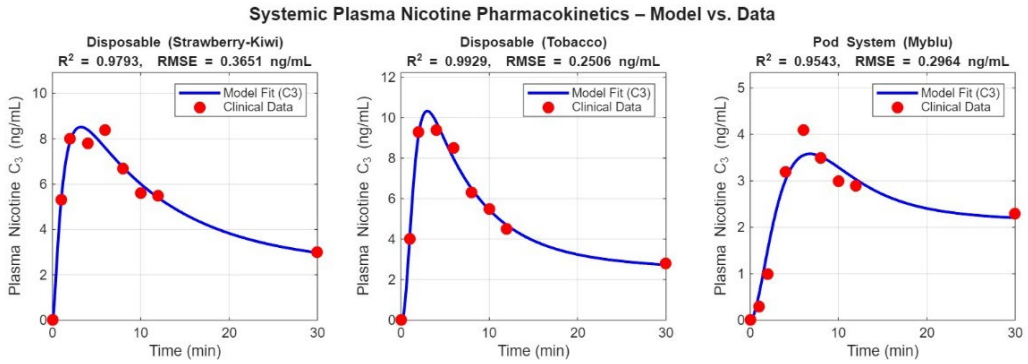


Figure 2. Systemic plasma nicotine pharmacokinetics: Comparison of Model Fit and Clinical Data Across Devices

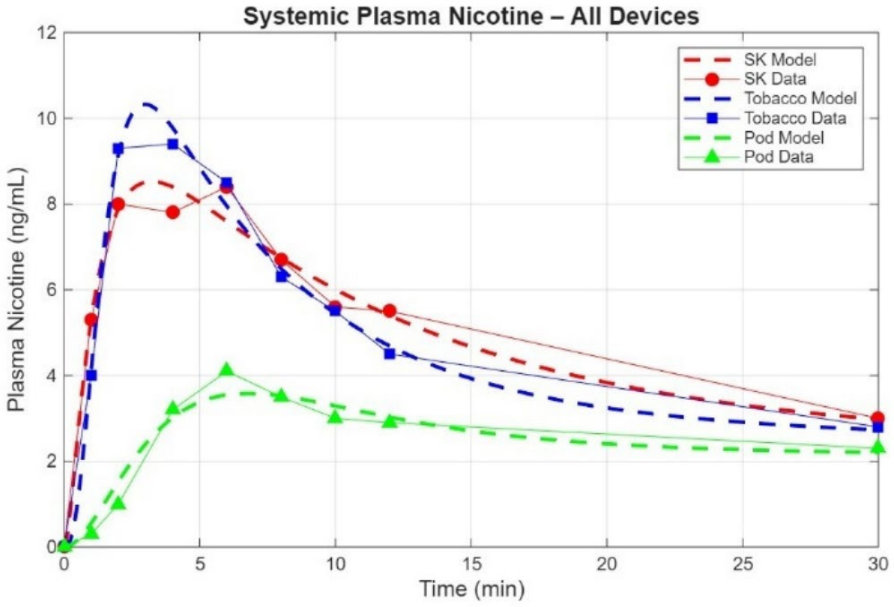


Figure 3. Systemic plasma nicotine concentration over time – Model Predictions and Clinical Data for All Devices

A noticeable difference between the devices was also observed in the pulmonary-to-systemic transfer parameter (k_{23}). The Strawberry-Kiwi disposable and the Pod system showed relatively higher transfer rates (k_{23} = 0.7896 and 0.5123 min^{-1}, respectively), suggesting more efficient nicotine movement from the pulmonary circulation into the systemic plasma compartment. In contrast, the Tobacco disposable device produced a much lower estimated value (k_{23} = 0.0100 min^{-1}). This result may indicate that nicotine transport in this device is less dependent on the pulmonary-to-systemic pathway and may

instead involve stronger transfer toward other compartments, particularly the brain pathway, as reflected by the relatively high estimated value of k_{24} = 2.1351 min^{-1}.

3.2 Plasma validation and theoretical multi-compartmental simulations

Following model calibration, the proposed ODE system was applied to generate exploratory simulations of nicotine concentration profiles in physiological compartments that were not directly measured in clinical study, including the lungs, pulmonary blood, brain, and liver. While the model demonstrated strong mathematical agreement with the observed clinical plasma nicotine data (as shown in Figures 2 and 3), the reconstructed tissue-level profiles in Figures 4-6 represent theoretical projections based on mathematical assumptions rather than validated physical measurements. These simulations are intended solely to provide a mechanistic framework for how nicotine might hypothetically distribute between different compartments over time and to compare device-specific transport kinetics under a uniform mathematical structure.

The simulated brain nicotine profiles (C_4) projected distinct kinetic trends among the three electronic cigarette platforms (Figures 4-6, upper panel: lung, pulmonary blood, and brain; lower panel: systemic plasma and liver). For the Strawberry-Kiwi disposable device (Figure 4), the high estimated pulmonary absorption rate (k_{12} = 5.0000 min^{-1}) resulted in a rapid calculated transfer from the lungs into pulmonary circulation, simulating a sustained mathematical accumulation in the brain compartment over time. The projected theoretical brain concentration reached approximately 21 ng/mL at 30 min. Under the model's assumptions, this accumulation pattern is mathematically driven by the slow simulated redistribution of nicotine out of the brain (k_{43} = 0.0155 min^{-1}) alongside continued influx from the systemic circulation (k_{34} = 0.0587 min^{-1}). Consequently, within the boundaries of this mathematical simulation, the Strawberry-Kiwi disposable device is projected to maintain a more prolonged tissue retention profile compared to the other systems.

In contrast, the Tobacco disposable device simulated a noticeably different exploratory profile for the brain compartment (Figure 5). Although the estimated pulmonary-to-brain transfer rate was high (k_{21} = 2.1351 min^{-1}), the simulated brain nicotine concentration exhibited a transient mathematical spike during the early phase and declined rapidly within the first five minutes, approaching near-baseline levels afterward. This rapid decrease is computationally associated with a high brain redistribution rate (k_{43} = 2.0000 min^{-1}), which mathematically routes nicotine out of the brain compartment in the model. Thus, the model suggests a short-duration but intense theoretical exposure pattern for the Tobacco disposable, differing substantially from the sustained retention simulated for the Strawberry-Kiwi device.

The Pod system (Myblu, Figure 6) generated the most gradual simulated brain profile among the three platforms. The lower calculated pulmonary absorption rate (k_{12} = 0.5291 min^{-1}) combined with a small pulmonary-to-brain transfer rate (k_{34} = 0.0100 min^{-1}) resulted in a slower simulated rise in brain nicotine concentration, mathematically approaching a plateau of approximately 7.5 ng/mL during the 20–30 minutes period. Additionally, a low redistribution rate (k_{43} = 0.0100 min^{-1}) maintained this stable simulated baseline. Compared to the disposable devices, the pod system was projected to exhibit a more moderate distribution trend within this compartment.

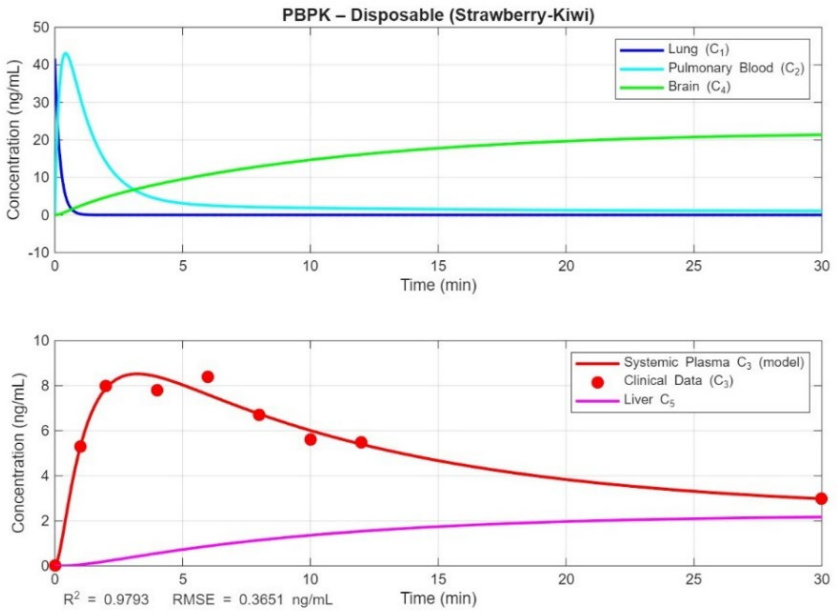


Figure 4. Predicted multi-compartmental nicotine distribution dynamics for Disposable E-cigarette (Strawberry-Kiwi flavor)

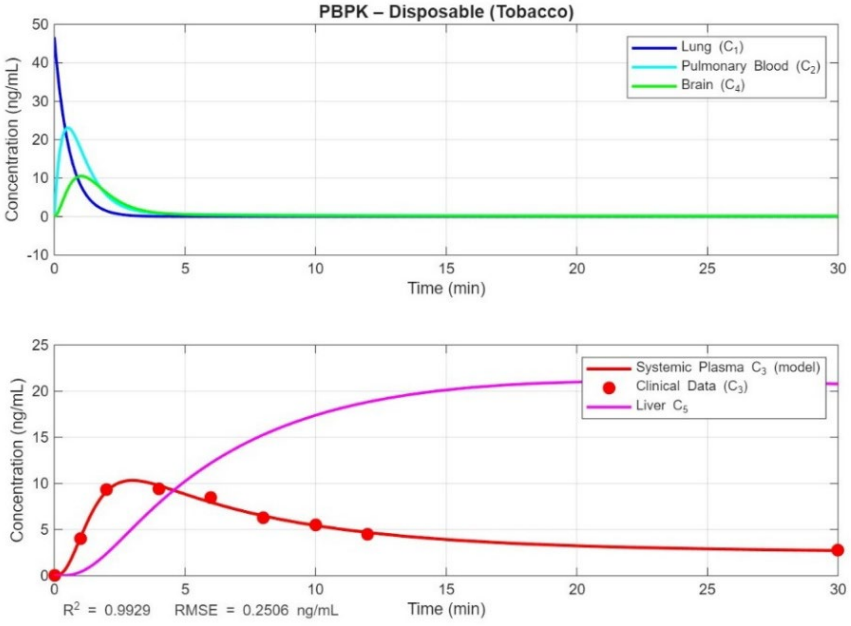


Figure 5. Predicted multi-compartmental nicotine distribution dynamics for isposable E-cigarette (Tobacco flavor)

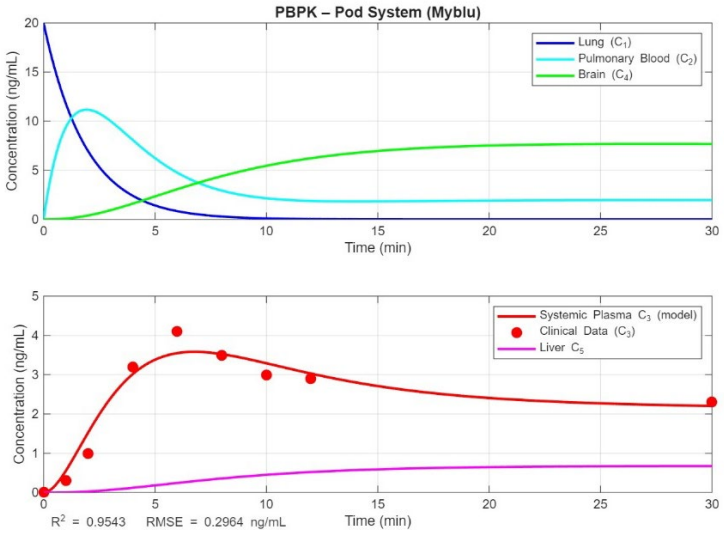


Figure 6. Predicted multi-compartmental nicotine distribution dynamics for Pod System E-cigarette (Myblu)

The simulated liver nicotine profiles (C_5) also projected varied theoretical trends. The Tobacco disposable device (Figure 5) generated the highest mathematical accumulation in the liver, with calculated concentrations increasing continuously to approximately 21 ng/mL at 30 min, occurring inversely to the simulated declines in plasma and brain concentrations. This calculated pattern is driven by the relatively high hepatic uptake rate (k_{35} = 0.1322 min^{-1}), suggesting a theoretical distribution bias toward hepatic pathways within this specific model configuration. Conversely, the Strawberry-Kiwi disposable and the pod systems (Figures 4 and 6) simulated substantially lower mathematical accumulation in the liver compartment, reaching projected concentrations of approximately 2.1 and 0.7 ng/mL at 30 min, respectively, due to the minimal hepatic uptake rate parameter assigned by the model (k_{35} = 0.0100 min^{-1}).

All three electronic cigarette platforms simulated rapid nicotine depletion from the lung compartment following the initial inhalation phase, reflecting the fast transport behavior typically assumed for nicotine salt aerosols. The Strawberry-Kiwi disposable device showed the fastest calculated pulmonary clearance (k_{12} = 5.0000 min^{-1}), with lung concentrations approaching near-zero levels within approximately 1 min, while the Tobacco disposable (k_{12} = 1.7330 min^{-1}) and the Pod system (k_{12} = 0.5291 min^{-1}) exhibited progressively slower simulated depletion patterns.

Overall, while these simulation results mathematically imply that differences in electronic cigarette design could influence internal nicotine distribution, these target organ profiles remain strictly exploratory and unvalidated due to the absence of direct clinical tissue data. By grounding the systemic plasma compartment in actual clinical measurements, this ODE framework offers a quantitative, hypothesis-generating tool to explore multi-compartmental kinetics; however, definitive toxicological or physiological exposure conclusions regarding the brain and liver cannot be verified without empirical tissue-level validation.

3.3 Parameter sensitivity and system robustness

To systematically evaluate the mathematical stability and robustness of the five-compartment framework, a local sensitivity analysis was conducted by perturbing the key unobserved tissue transfer rates—specifically the pulmonary absorption rate (k_{12}) and the brain transport rates k_{24} , k_{42} , k_{34} , and k_{43})—by ±20% from their optimized baseline values. The impact of these variations on the central plasma nicotine concentration (C_3) was evaluated.

The simulations revealed that the model's peak plasma profile exhibits a high degree of mathematical stability in terms of the primary pulmonary absorption rate (k_{12}). A 20% decrease in k_{12} marginally delayed the plasma time-to-peak ($T_{\max}$) from 3.67 to 3.73 min} (a delay of 0.06 min) and reduced the maximum concentration ($C_{\max}$) by approximately 0.13% (from 7.8521 to 7.8422 ng/mL). This indicates that while k_{12} governs the primary initial entry, the global peak concentration is mathematically well-buffered against localized perturbations at this baseline configuration.

Conversely, when the peripheral brain transport parameters k_{24} , k_{42} , k_{34} , and k_{43}) were perturbed simultaneously by ±20% , the global plasma concentration curve exhibited a maximum deviation of 12.96%. While this target organ perturbation introduces a noticeable quantitative shift in the plasma profile, the overall dynamic shape, uptake trajectory, and elimination phases of the curve remain structurally stable without causing numerical divergence or mathematical destabilization. This sensitivity behavior demonstrates that while parameter uncertainties within the unobserved brain compartment can influence systemic plasma levels to a certain degree, the calibrated plasma fits maintain structural identifiability and consistent pharmacokinetic trends (as illustrated in Figure 7).

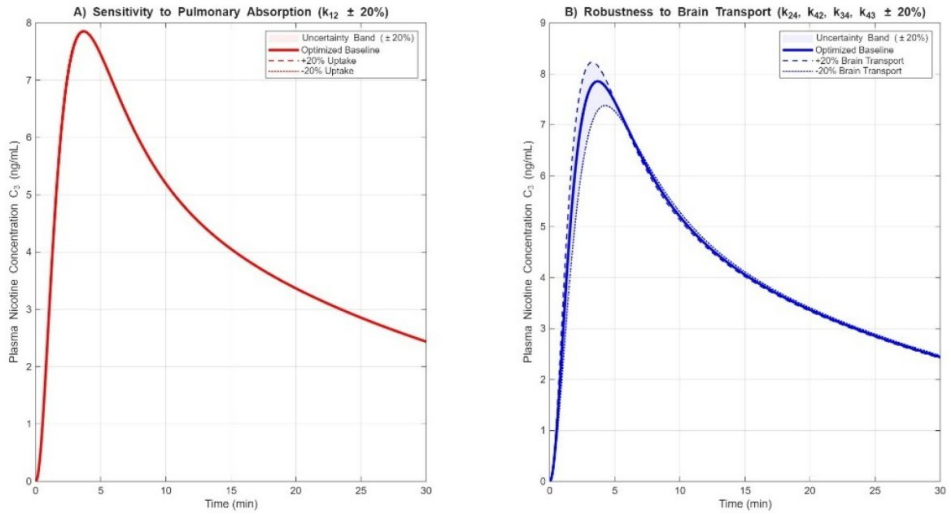


Figure 7. Local sensitivity analysis and structural robustness of the central plasma concentration (C_3) under a ±20% parameter perturbation

4. Conclusions

This study successfully established a five-compartment ordinary differential equation model to simulate nicotine pharmacokinetics following electronic cigarette use. The model demonstrated high mathematical accuracy and robustness in replicating clinical plasma nicotine profiles across three different device platforms. Furthermore, parameter sensitivity analysis confirmed the structural stability and identifiability of the calibrated framework, demonstrating that the central circulation kinetics remain highly stable even when subjected to peripheral parameter uncertainties.

Regarding target organ exposure, the model was utilized to simulate theoretical nicotine dynamics in unobserved tissues, including the lungs, brain, and liver. Based on these mathematical simulations, the results suggest distinct regional distribution patterns and varying peak concentration times across device types, reflecting potential differences in delivery efficiency. However, because direct empirical validation within human target organs is unattainable due to the lack of external peer-reviewed tissue data and ethical sampling limitations, these tissue-specific profiles must be treated strictly as exploratory, hypothesis-generating estimations rather than definitive measurements. Overall, while the model offers valuable mathematical insights into the systemic distribution behavior of nicotine salts, caution must be exercised when extrapolating these simulations to absolute organ-level exposure or clinical risk assessments.

Despite its utility, a key limitation of this five-compartment model is the simplification of complex perfusion dynamics into first-order kinetic transfer rates. Furthermore, because several compartments (e.g., lung, brain, and liver) remain unobserved clinically, parameter estimation relies heavily on central plasma data, posing inherent identifiability challenges unless constrained by established physiological literature. To address these limitations, several directions may further improve the current framework. First, future studies should incorporate cotinine dynamics to investigate longer-term nicotine metabolism and clearance beyond the acute exposure phase. Second, aerosol physicochemical properties, such as particle size and aerosol pH, could be linked directly to the pulmonary absorption parameter (k_{12}) to improve predictions for newer nicotine formulations. Third, the model could be extended to simulate repeated puffing sessions to evaluate nicotine accumulation during habitual use. Finally, nonlinear mixed-effects modeling (NLME) could be incorporated to account for inter-individual variability in metabolism, inhalation behavior, and device usage patterns.

5. Acknowledgements

The author gratefully acknowledges the researchers whose clinical data were utilized in this study, particularly those contributing to the referenced Phase I investigation, for providing essential data that enabled model development and validation.

6. Authors' Contributions

Thanachok Mahahong conceived and designed the study, performed the research, analyzed the data, and wrote the manuscript.

ORCID

Thanachok Mahahong https://orcid.org/0009-0003-1878-4237

7. Conflicts of Interest

The author declares no conflict of interest.

8. AI Declaration

AI tools (ChatGPT, OpenAI; Claude, Anthropic) were used to assist with language refinement and consistency checking. All content has been reviewed and edited by Thanachok Mahahong, who takes full responsibility for the accuracy, integrity, and scientific content of this publication.

References

Aster, R. C., Borchers, B., & Thurber, C. H. (2018). *Parameter estimation and inverse problems* (3rd ed.). Academic Press.

Benowitz, N. L., Hukkanen, J., & Jacob, P. (2009). Nicotine chemistry, metabolism, kinetics and biomarkers. In J. E. Henningfield, E. D. London, & S. Pogun (Eds.), *Nicotine Psychopharmacology* (pp. 29-60). Springer. https://doi.org/10.1007/978-3-540-69248-5_2

Davies, B., & Morris, T. (1993). Physiological parameters in laboratory animals and humans. *Pharmaceutical Research, 10*(7), 1093-1095. https://doi.org/10.1023/a:1018943613122

Falarowski, C., Pieper, E., Rabenstein, A., Mallock-Ohnesorg, N., Burgmann, N., Franzen, K., Gertzen, M., Koller, G., Nowak, D., Rahofer, A., Rieder, B., Roselli de Oliveira Pinto Kise, G., Schulz, T., Strohmeyer, E., Laux, P., Luch, A., & Rüther, T. (2025). Disposable e-cigarettes and their nicotine delivery, usage pattern, and subjective effects in occasionally smoking adults. *Scientific Reports, 15*(1), Article 16270. https://doi.org/10.1038/s41598-025-97491-5

Godfrey, K. (1983). *Compartmental models and their application*. Academic Press.

Hajek, P., Pittaccio, K., Pesola, F., Myers Smith, K., Phillips-Waller, A., & Przulj, D. (2020). Nicotine delivery and users' reactions to Juul compared with cigarettes and other e-cigarette products. *Addiction, 115*(6), 1141-1148. https://doi.org/10.1111/add.14936

Hindmarsh, A. C., Brown, P. N., Grant, K. E., Lee, S. L., Serban, R., Shumaker, D. E., & Woodward, C. S. (2005). SUNDIALS: Suite of nonlinear and differential/algebraic equation solvers. *ACM Transactions on Mathematical Software, 31*(3), 363-396. https://doi.org/10.1145/1089014.1089020

Hukkanen, J., Jacob, P., & Benowitz, N. L. (2005). Metabolism and disposition kinetics of nicotine. *Pharmacological Reviews, 57*(1), 79–115. https://doi.org/10.1124/pr.57.1.3

Jacquez, J. A. (1996). *Compartmental analysis in biology and medicine* (3rd ed.). BioMedware.

Kovar, L., Selzer, D., Britz, H., Benowitz, N., St. Helen, G., Kohl, Y., Bals, R., & Lehr, T. (2020). Comprehensive parent–metabolite PBPK/PD modeling insights into nicotine replacement therapy strategies. *Clinical Pharmacokinetics, 59*(9), 1119-1134. https://doi.org/10.1007/s40262-020-00880-4

National Academies of Sciences, Engineering, and Medicine. (2018). *Public health consequences of e-cigarettes.* The National Academies Press. https://doi.org/10.17226/24952

O'Connell, G., Pritchard, J. D., Prue, C., Thompson, J., Verron, T., Graff, D., & Walele, T. (2019). A randomised, open-label, cross-over clinical study to evaluate the pharmacokinetic profiles of cigarettes and e-cigarettes with nicotine salt formulations

in US adult smokers. *Internal and Emergency Medicine, 14*(6), 853-861. https://doi.org/10.1007/s11739-019-02025-3

Price, K., Haddad, S., & Krishnan, K. (2003). Physiological modeling of age-specific changes in the pharmacokinetics of inhaled substances. *Journal of Toxicology and Environmental Health, Part A, 66*(5), 417-433. https://doi.org/10.1080/15287390306450

Prochaska, J. J., & Benowitz, N. L. (2019). Current advances in research in treatment and recovery: Nicotine addiction. *Science Advances, 5*(10), Article eaay9763. https://doi.org/10.1126/sciadv.aay9763

Raue, A., Kreutz, C., Maiwald, T., Bachmann, J., Schilling, M., Klingmüller, U., & Timmer, J. (2009). Structural and practical identifiability analysis of intracellular signaling pathways by means of profile likelihood. *Bioinformatics, 25*(15), 1923-1929. https://doi.org/10.1093/bioinformatics/btp358

Robinson, R. J., Eddingsaas, N. C., DiFrancesco, A. G., Jayasekera, S., & Hensel, E. C., Jr. (2018). A framework to investigate the impact of topography and product characteristics on electronic cigarette emissions. *PLoS ONE, 13*(11), Article e0206341. https://doi.org/10.1371/journal.pone.0206341

Rostami, A. A., Campbell, J. L., Pithawalla, Y. B., Pourhashem, H., Muhammad-Kah, R. S., Sarkar, M. A., Liu, J., McKinney, W. J., Gentry, R., & Gogova, M. (2022). A comprehensive physiologically based pharmacokinetic (PBPK) model for nicotine in humans from using nicotine-containing products with different routes of exposure. *Scientific Reports, 12*(1), Article 1091. https://doi.org/10.1038/s41598-022-05108-y

St. Helen, G., Havel, C., Dempsey, D. A., Jacob, P., & Benowitz, N. L. (2016). Nicotine delivery, retention, and pharmacokinetics from various electronic cigarettes. *Addiction, 111*(3), 535-544. https://doi.org/10.1111/add.13183

Talih, S., Salman, R., Soule, E., El-Hage, R., Karam, E., Karaoghlanian, N., El-Hellani, A., Saliba, N., & Shihadeh, A. (2022). Electrical features, liquid composition and toxicant emissions from 'pod-mod'-like disposable electronic cigarettes. *Tobacco Control, 31*(5), 667-670. https://doi.org/10.1136/tobaccocontrol-2020-056362

Yamazaki, H., Horiuchi, K., Takano, R., Nagano, T., Shimizu, M., Kitajima, M., Murayama, N., & Shono, F. (2010). Human blood concentrations of cotinine, a biomonitoring marker for tobacco smoke, extrapolated from nicotine metabolism in rats and humans and physiologically based pharmacokinetic modeling. *International Journal of Environmental Research and Public Health, 7*(9), 3406-3421. https://doi.org/10.3390/ijerph7093406

Yingst, J. M., Foulds, J., Veldheer, S., Hrabovsky, S., Trushin, N., Eissenberg, T. T., Williams, J., Richie, J. P., Nichols, T. T., Wilson, S. J., & Hobkirk, A. L. (2019a). Nicotine absorption during electronic cigarette use among regular users. *PLoS ONE, 14*(7), Article e0220300. https://doi.org/10.1371/journal.pone.0220300

Yingst, J. M., Hrabovsky, S., Hobkirk, A., Trushin, N., Richie, J. P., & Foulds, J. (2019b). Nicotine absorption profile among regular users of a pod-based electronic nicotine delivery system. *JAMA Network Open, 2*(11), Article e1915494. https://doi.org/10.1001/jamanetworkopen.2019.15494

Ynineb, A. R., Yumuk, E., Copot, D., Ayvaz, B., Khoumeri, B., Ben Othman, G., Mihai, M. D., Birs, I. R., Muresan, C. I., & Ionescu, C. M. (2025). Modeling drug retention as memory effects in obese patients using fractional and augmented models. *Scientific Reports, 15*(1), Article 26234. https://doi.org/10.1038/s41598-025-10172-1